Automatic inspection for surface imperfections: requirements, potentials and limits

Ralph Neubecker, Jenny E. Hon

Fachbereich Mathematik und Naturwissenschaften, Darmstadt University of Applied Sciences, Schöfferstr.3, 64295 Darmstadt. email: ralph.neubecker@h-da.de

ABSTRACT

The inspection of optical elements for surface imperfections is mostly based on subjective evaluation by human operators. Automatic inspection systems (AIS) may introduce advantages in term of reliability, reproducibility and cycle time. The potential and limits of a camera-based, high-resolution AIS for scratches and digs are discussed. One important aspect is the illumination concept (brightfield or darkfield), regarded in relation to the scattering properties of an imperfection. Another aspect is the achievable spatial resolution of such a system. Different resolution limiting factors are considered, leading to criteria for the choice of digital sensors und imaging optics. Options to overcome a limited depth-of-field are also outlined. Next to technical aspects, the role of related standard specifications and system validations are addressed.

Keywords: surface imperfections, scratch and dig, automatic inspection

1. INTRODUCTION

1.1 Context

One important quality feature of optical elements is the presence of surface imperfections, like scratches and digs. Often, such defects are only ‘cosmetic’ in nature, in the sense that they rarely affect the optical performance[1,2,3]. Nevertheless, they attract customer's attention and indicate deficiencies in the manufacturing process. Only in the case of laser optics, surface imperfections cause indeed functional constraints, either by inducing intra-cavity losses or by initiating laser-induced damage. As consequence, an inspection for such imperfections is commonly required for all precision optics.

Typically, the corresponding inspection process is still based on subjective appraisal of human operators. Even actual standardization documents specify mainly human inspection. Human operators are unsurpassed concerning their flexibility and an intelligent application of testing rules. However, the achievable pace is limited and it is problematic that the individual decision criteria may vary in time and may differ between operators.

In times of automated production and with respect to the capabilities of modern machine vision systems, one may raise the question if automatic, camera-based inspection systems (AIS) could be utilized. In 100%-inspection tasks in mass production, the short cycle time would be beneficial. The good repeatability of an AIS could potentially provide reliable test references, even for offline-systems. Finally, AIS easily generate digital documentation of all defects found on each individual sample, as well as statistics over many samples. One use of this lies in more efficient control of the manufacturing process. Some systems had been described in the recent years[3,4,5,6,7], only few are commercially available today. Still, it appears that they have not (yet) found broad acceptance. The availability of new image processing hardware, and a critical reflection of the inspection process and the underlying standards may open new opportunities here.

The visual inspection includes the use of different illuminations, possibly the use of scale magnifiers and the manual tilt and turning of the optical component. This could in principle be replicated with several cameras with different magnifications, and motorized positioning systems. Mechanical actuators are slow and require more maintenance than a fixed digital camera. Therefore, a high resolution AIS is more attractive, capable to test a sample with a single snap shot, avoiding further motion, alignments or changes in optical magnification.

Third European Seminar on Precision Optics Manufacturing, edited by Rolf Rascher, Oliver Fähnle, Christine Wünsche, Christian Schopf, Proc. of SPIE Vol. 10009, 1000907 · © 2016 SPIE
CCC code: 0277-786X/16/$18 · doi: 10.1117/12.2235863

1.2 Constituents of Automatic Inspection Systems

Any Automatic Inspection System will consist of a light source, providing the illumination, the sample with the imperfection itself, and a camera, registering light scattered by the imperfection. The relative arrangement of light source, sample and camera with respect to each other, as well as the angular distribution of the illuminating radiance and the acceptance angle of the imaging optics define, whether the imperfection is detected in brightfield or in darkfield conditions. The digital image, as recorded by a digital camera, can be processed by a computer to detect and grade possible imperfections. Except for the latter, an AIS is directly comparable to inspection by human operators.

In this paper, the requirements for these AIS-constituents will be discussed. The focus will be on two questions: how can an optimal image contrast be achieved, such that image processing algorithms may reliably identify and measure imperfections? And which spatial resolution is attainable, e.g. can small imperfections be detected? Brightfield illumination will be compared to darkfield, in terms of image contrast and in terms of a signal-to-noise ratio, both with respect to the angular spectrum of the imperfection scattering distribution and the numerical aperture of the imaging optics. Different resolution-limiting factors will be regarded, from which constraints for the choice of image sensors and imaging optics are derived. As consequence of these constraints, one may end up with a small depth of field, leading to limitations for the inspection of curved surfaces. These limits may be overcome by image processing methods achieving an extended depth of field.

The paper will close with some remarks on aspects of validation and system acceptance. However, before going into technical details, we start with a look into regulatory aspects.

2. STANDARDS

The grading and classification of surface imperfections on optical elements, like scratches and digs, is defined in the international standard ISO 11010-7 [8], where imperfection grading is connected to their lateral geometric size. This standard is complemented by the ISO 14997, describing the necessary test method. It is mainly being based on visual inspection procedures to be carried out by human operators[9], using reference artefact for comparison.

The smallest size to be measured as geometrical extent according to ISO 14997 is 10 µm. This size will be taken as benchmark in the following for the AIS spatial resolution. The standard stipulates to grade smaller imperfections by the brightness of their visual appearances. Since their appearance in a digital image very much depends on the optical system design, the corresponding visibility grading is a question of image processing, which needs to be adapted to the particular AIS design.

Particularly in the US, the standard MIL-PRF 13830B plays a role [10]. It is also based on visual comparison of imperfections to artefacts. These artefacts are traced back to a primary reference target (*master standard*), and there is no well-defined relation to the imperfection size (although there had been extensive discussions on this possible relation[1,4]). Hence, the definitions laid down in the MIL-PRF 13830B do not provide a direct guideline for the design of an AIS. Nevertheless, the image processing software of a suitable AIS can probably be taught to perform a MIL-grading.

For grading of the imperfections, a limited number of grading classes is defined in the standards. Moreover, several rules are defined how a number of imperfections appearing on the optical element can be subsumed. Since implementing those grading rules should not pose a problem, the main challenge for designing an AIS is to precisely measure the size of small imperfections. When small imperfections can be detected, the grading of larger imperfections, like edge chips, will be easy.

Existing standards are mainly written as procedure rules for human operators. Here, the imaging system is given by the eye meaning that several optical parameters are fixed or can vary only in a limited range (focal length, F-number, working distance, resolution). The use of a technical imaging system opens new degrees of freedom, which may require corresponding regulations in future versions of the standards.

3. ILLUMINATION AND OBSERVATION

3.1 Sizing by image processing

Before turning to the optical appearance of imperfections under particular illumination conditions, let us first take a brief look at the end of the chain, the sensor signal and the image processing. Figure 1 shows an example for an imperfection observed under darkfield conditions, i.e. as bright object on dark background. When many pixels are covered (l.h.s.

graphs), sizing by image processing comes down to set an appropriate threshold and count the number of pixels above threshold. In order to do so, the imperfection signal needs to be well above background noise.

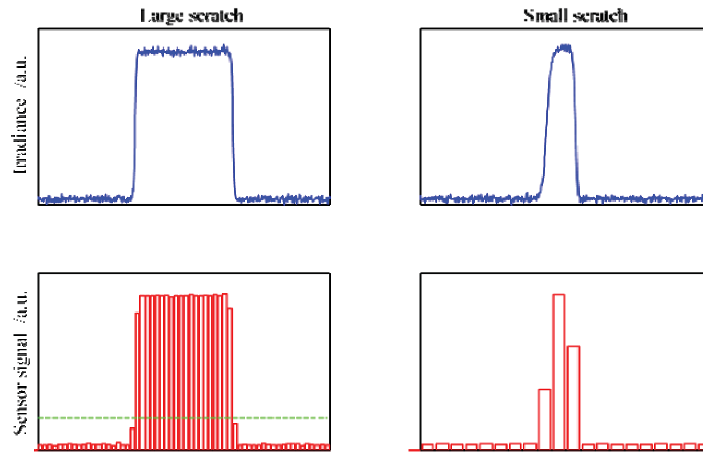

Figure 1: Linear profiles from an imperfection in darkfield conditions, top: irradiance in the image, bottom: resulting sensor signal. L.h.s.: large imperfection, covering many sensor pixels, r.h.s.: small imperfection covering few pixels

For small imperfections, covering only few pixels (r.h.s. graphs), some of the pixels are only partially covered and the resulting sizing uncertainty of ± 1 pixel may become too large. In this case, it is reasonable to also utilize the signal levels of the corresponding pixels to estimate the size. This kind of radiometric sizing is similar to the visibility of an imperfection to a human operator. Figure 1 also illustrates a rule of thumb in image processing, which says that one needs at least 2 pixels to detect an object. Consequently, with our benchmark of 10 µm, a pixel should cover at least 5µm on the sample to be inspected.

3.2 Optical appearance of surface imperfections

Surface imperfections scatter light because of the topography of the glass-air surface; it is a feasible assumption that there is no absorption process (at least in the linear regime). Such scattering can fully be described by diffraction theory. Rigorous approaches take the boundary conditions of the light field into consideration, accounting for a transmission / reflection coefficient, depending on the local surface angle[11,12,13,14]. The model can be completed by averaging over the illumination spectrum, when incoherent, polychromatic light is used.

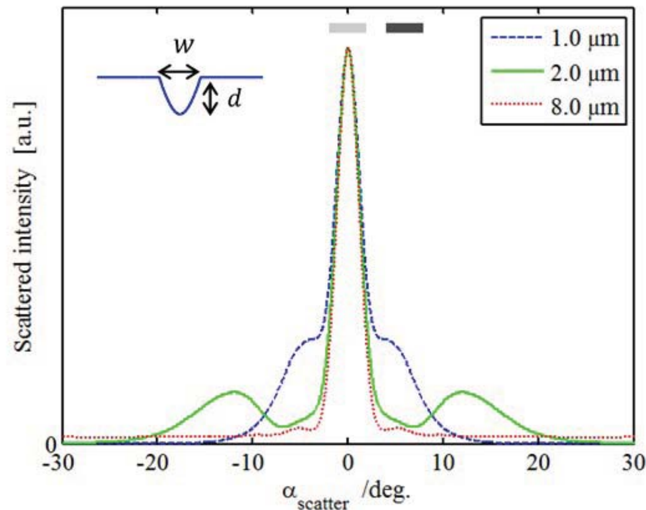

Figure 2: Simulated scatter distribution for a 10 μm wide scratch versus scatter angle, with scratch depth d as parameter. The inset shows the scratch profile. The light and dark gray bars on top of the curves indicate the acceptance angles of the imaging optics under brightfield and under darkfield conditions, respectively.

The scattering distribution (scattered radiance as function of scatter angle) sensitively depends on the imperfection topography. This topography will not only depend on the cause for the imperfection (polishing, handling …), but also on the particular manufacturing process. Even scratches caused by the same cause, namely by rogue particles in polishing processes, may already differ substantially one from another[15]. Hence, even though all theoretical tools are at hand, it is almost impossible to derive general statements on scatter distributions for surface imperfections.

Diffraction theory says that the scatter angles $\alpha_{scatter}$ scale with the transverse structure size w by $\sin\alpha_{scatter} \sim \lambda/w$. For a smooth surface profile, w is given by the dig diameter, or the scratch width respectively. However, imperfections with a complex, rough microstructure cause much larger scatter angles. Besides, the imperfection depth also plays a role for the scatter distribution, like the scattering at a particle is determined by its volume and not only by its cross section[14]. In terms of inspection, this means that the visibility of an imperfection is not only determined by its geometric extension, but also by its microstructure and its depth.

The simulated scattering distribution, which is used for illustration in the following, is computed for a smooth scratch (sleek) with a cosine-profile (see Figure 2). In this one-dimensional case, light will only be deflected in the direction perpendicular to the scratch long axis. Assuming white light illumination, the fine modulations in the scatter distribution are lost by averaging over the spectrum. Another effect of real light sources results from their angular radiance distribution, which will be convolved with the scattering distribution of the imperfection. For simplicity, perfectly collimated light was assumed here.

Even in this simple model, the scattering distribution significantly changes with scratch depth, sometimes leading to distinct side lobes[13]. A particular relation between the amplitudes of the side lobes and the scratch depth and width can, however, only be deduced for a well-known scratch topography.

3.3 Brightfield and darkfield configuration

In many optical inspection tasks, one has the basic choice between brightfield and darkfield observation, as schematically shown in Figure 3. Even though the illustration refers to observation in transmission, the same arguments hold for observation of reflected light.

In brightfield, interesting entities, like surface imperfections, are recorded as dark objects on a bright background. Often, this results from looking into the illumination source (possibly through a reflection on the sample surface), with the imperfections scattering light out of the imaging path. In contrast, under darkfield conditions imperfections appear as bright objects on a dark background. Here, the imperfections scatter light into the imaging path, while the illumination is not imaged onto the sensor.

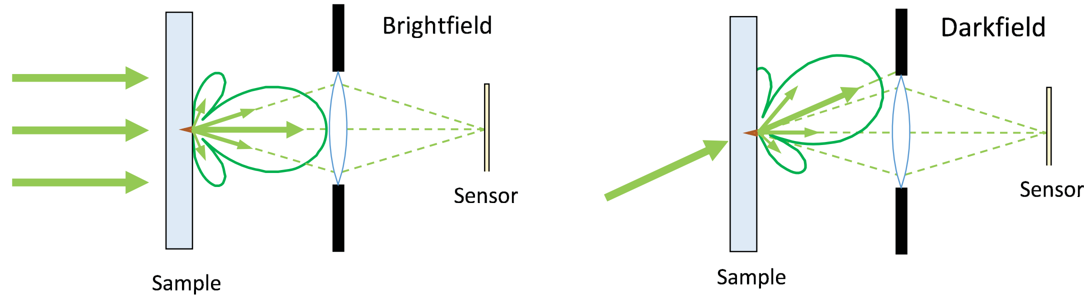

Figure 3: Location of the imaging optics with respect to the scattering lobe, caused by the imperfection. L.h.s.: in brightfield, the imaging optical axis coincides with the illumination direction. R.h.s.: in darkfield, the illumination is blocked, only scattered light reaches the sensor.

For the purpose of the size measurement of imperfections, both illumination concepts are useful, as the main objective is to identify the border of the imperfection. When it comes to determining the radiometric equivalent size instead, there are indeed differences between darkfield and brightfield.

In the present context, we will regard the imaging of imperfections onto digital camera sensors. The signal from a pixel covered by the image of an imperfection is determined by the scattering properties of the imperfection, determining the (angular) distribution of the scattered light. The difference between brightfield and darkfield configuration lies in the location of the aperture of the imaging system (gray horizontal bars in Figure 2). In brightfield conditions, the aperture captures only the central part of the scattering distribution (around zero scattering angle), while in darkfield, the aperture captures parts of the scattering outside the forward direction.

This already makes clear that for a high image contrast in brightfield, the numerical aperture should be chosen to be small. Whereas darkfield would require a large aperture, ideally placed in the direction the dominant scattering side lobe. With the eye as detector, the numerical aperture is indeed quite small, making brightfield in principle adequate for visual inspection. However, using camera systems, small apertures are not desirable.

3.4 Image contrast

The detectability of an imperfection will in general depend on the contrast between the image of the imperfection and the background. In darkfield, real background-light will be generated by residual surface scattering of the sample itself, or by remaining reflectance of blackout material behind the sample. Not being within the scope of the AIS itself, such background light will be assumed to be negligible.

Contrast is usually defined as $M = (S_{max} - S_{min})/(S_{max} + S_{min})$, where we here refer to sensor signals S, which are proportional to the corresponding irradiance on the sensor and may e.g. be measured in units of gray levels (Digital Numbers, DN). S_{max} and $S_{min}$are the maximum and minimum signal, respectively, found in the region around the imperfection's image. Correspondingly, for darkfield, S_{max} is the signal belonging to the imperfection and S_{min} belongs to the background, while vice versa holds for brightfield.

The irradiance at the imperfection's image is governed by the amount of scattered light, being captured by the imaging optics in the case of darkfield, or not being captured in the case of brightfield respectively. Hence, this irradiance depends on the imperfection's scatter distribution, and the location and size of the imaging aperture. For simplicity, these contributions are summarized[4] in a single *scattering magnitude* κ. The corresponding sensor signal follows as $|S_{imp}| \sim \kappa \cdot S_I$, where S_I is the signal belonging to the illuminating irradiance, and $0 \leq \kappa \leq 1$. Since only a small part of the scattered light is collected by the imaging optics, the darkfield scattering magnitude $\kappa_{DF} \ll \kappa_{BF}$ is in general smaller than the one for brightfield. Note that this can be balanced by using a larger illumination irradiance in darkfield, since the illuminating light is not imaged onto the sensor.

Under brightfield conditions, the imperfection signal reads as $S_{imp} = (1 - \kappa_{BF}) \cdot S_I + S_{cam}$ and the bright background is $S_{back} = S_I + S_{cam}$. For completeness, we also include a signal offset S_{cam} generated by the camera. Setting $S_{max} = S_{back}$ and $S_{min} = S_{imp}$, we arrive at a brightfield contrast of

$$M_{BF} = \frac{\kappa_{BF}}{2\,(1+S_{cam}/S_I)-\kappa_{BF}} \approx \frac{\kappa_{BF}}{2-\kappa_{BF}}, \tag{1}$$

ranging between $0 \le M_{BF} \le 100\%$, depending on the scattering magnitude κ_{BF}.

For darkfield, we take $S_{imp} = \kappa_{DF} \cdot S_I + S_{cam}$ and $S_{back} = S_{cam}$, leading to

$$M_{DF} = \frac{1}{1+2\,S_{cam}/(\kappa_{BF}S_I)} \approx 1. \tag{2}$$

When all sensor signals are offset-corrected ($S_{cam} \to 0$), darkfield contrast is always 100%.

An illustrative example of the dependences of sensor signal and contrast on the imaging NA is illustrated in Figure 4, which is based on the 1-dimensional simulation shown in Figure 2 (10 µm wide and 2 µm deep scratch). The larger the numerical aperture is chosen in the case of brightfield, the more scattered light is captured, until finally the image of the scratch has the same signal level as the background. Accordingly, the contrast drops. When comparing to Figure 2, the effect of capturing the distinct side lobe at $\pm 12°$ can be recovered at $NA \approx 0.2$. The decrease in contrast with numerical aperture will be more prominent for imperfections with larger structures, which cause tighter scattering lobes.

For a numerical aperture of $NA \approx 0.1$, large enough to avoid diffraction limitations in resolution (see below), the resulting brightfield contrast in this example is just about 30%. Even for small values of $NA \approx 0.01$, as mentioned in the ISO 14997 and related to the conditions given by observation with the naked eye, contrast is already only ~70%.

For darkfield, the basic tendency is the opposite: the larger the numerical aperture, the larger the signal level becomes. As soon as the imaging aperture starts to capture the illumination (at NA$\approx$ 0.28), the signal rises steeply – but now the darkfield condition is violated. Contrast is not shown in the darkfield graph, as (for this idealized simulation) it remains at a constant value of 100%. However, the darkfield signal sensitively depends on the angular location of the imaging optics with respect to the angular scattering distribution. From Figure 2 it can be taken that with the indicated location of the imaging aperture (dark bar), the prominent side lobe of the 2 µm deep scratch would not be captured, while the 1 µm deep scratch would generate a noticeable signal.

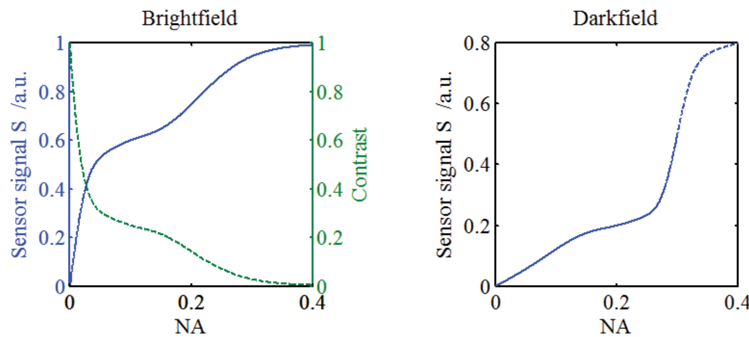

Figure 4: L.h.s.: Simulated example for the dependence of the brightfield signal and image contrast (dashed curve) on the imaging optics numerical aperture NA. R.h.s.: Darkfield signal vs NA.

Figure 5 shows examples of experimentally found signal levels and contrasts under variation of the aperture. The examined scratch is significantly larger (~80 µm wide) than the one considered in the above simulations, but has some microstructure. Also the covered the NA-range is much smaller and the illumination is not perfectly collimated. Nevertheless, the tendency is the same as in the simulations: for brightfield, the signal level increases when the aperture is opened, with the consequence of dropping contrast. The darkfield signal also increases with NA, and the measured contrast remains close to 100%.

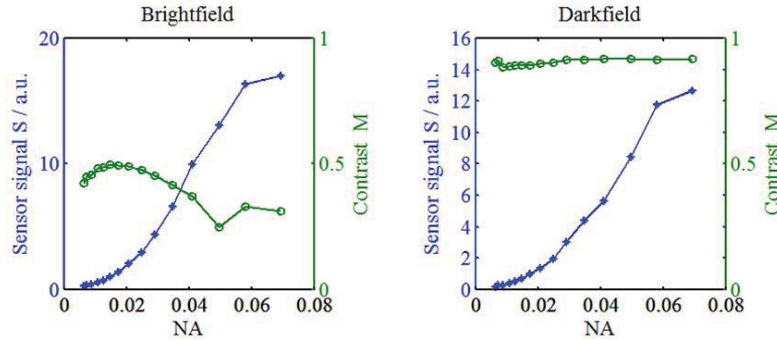

Figure 5: Experimentally determined sensor signals (o-o) from an imperfection under variation of the imaging optics aperture, together with resulting contrast (*-*). Brightfield is shown in the l.h.s. graph, darkfield in the r.h.s. graph.

In general, the optimum location of the imaging optics in a darkfield configuration would change from imperfection to imperfection. Even worse, the present 1D model ignores the azimuthal angle. Digs will generate a rotationally symmetric scatter distribution. Instead, (ideal) scratches scatter light mainly into a direction perpendicular to their long axis. If the imaging axis is not in this direction, the scratch will be (almost) invisible. Such effects are probably quite familiar to all operators and are the reason why the samples are turned and tilted during inspection. Reproducing this practice (e.g. by using actuators) is just as unattractive for an AIS-design as moving the camera around. The way out is to change location of the illumination source instead or to use an extended illumination.

3.5 Signal and noise

Contrast does not take noise into account, which however does play a role in the detection of an imperfection by an image processing algorithm. Noise in camera sensor signals originates from several sources, the main contributions result from electronic read-out noise and statistical variations of the dark signal. The statistic variations in photon numbers (shot noise) represent the other important noise source – always present and not related to the sensor[16].

With respect to detection by image processing, we compare the average signal S_{imp} of pixels, onto which an imperfection is imaged, to adjacent pixels, where we regard background signal and background noise. To quantify this, we define a *Signal-to-background-noise ratio*

$$SBNR = \frac{|S_{imp} - S_{back}|}{\sigma_{back}}, \tag{3}$$

where S_{back} is the background signal, $|S_{imp} - S_{back}|$ is the net imperfection signal and σ^2_{back} is the corresponding signal variance (noise).

For low irradiance values, the camera-specific electronic noise dominates $\sigma^2_{back} \approx \sigma^2_{cam}$, while photon noise dominates for large irradiance $\sigma^2_{back} \approx \sigma^2_{phot}$. Photon noise follows the Poisson distribution, i.e. the variance is proportional to the total photon number $\sigma^2_{phot} = \mathrm{QE} \cdot N_{phot}$, with the photon number N_{phot} incident onto the sensor pixel during integration time. QE denotes the pixel quantum efficiency in converting incoming photons to charge carriers. The sensor signal $S = k\, QE\, N_{phot} + S_{cam}$ also depends on the sensor gain k, e.g. measured in V/e^- and the signal offset S_{cam} results from sensor dark current.

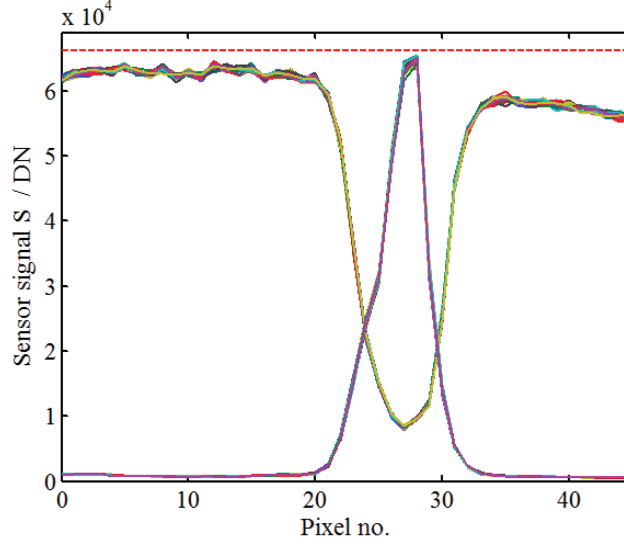

Figure 6: Experimentally found signal profiles for a large scratch under brightfield and under darkfield conditions. The graph consist of an overlay of 48 curves, taken from subsequent images in order to illustrate temporal noise.

A comparison of brightfield and darkfield observation of an imperfection is schematically shown in Figure 6. These linear signal profiles are taken from images recorded with a 14-bit matrix camera. One general restriction of imaging sensors is that the signal $S \leq S_{sat}$ is limited by a saturation limit (Full Well Capacity, dashed horizontal line in Figure 6. Hence, both graphs represent the situation of reaching almost the maximum of the achievable contrast.

The graphs in Figure 6 are overlays of 48 curves, taken from subsequent images, indicating variations due to the temporal noise. Additionally, there is some stationary spatial variation originating from residual surface scatter from the sample. As expected, the noise amplitude is larger for large signal amplitudes. In the present case, the background noise level is $\sigma_{back} \cong 38$ digital numbers (DN) for darkfield, and $\sigma_{back} \cong 300$ DN for brightfield. The resulting signal-to-background-noise ratios are $SBNR_{DF} = 1700$ for darkfield, and $SBNR_{BF} = 185$ for brightfield, respectively. For such large $SBNR$ values, noise will of course not really interfere with the detection of the imperfection. This will be different for less prominent imperfections, leading to a sensor signal in the order of the background noise amplitude ($SNBR \gtrsim 1$).

General expressions can be derived using the above expressions. For the brightfield case we arrive at

$$\left|S_{imp} - S_{back}\right| = \kappa_{BF}\, S_I = \kappa_{BF}\, K\, QE\, N_I \,. \tag{4}$$

N_I is the photon number corresponding to the illumination irradiance S_I, which also determines the noise on the adjacent background pixels $\sigma_{back}^2 \approx K^2\, QE\, N_I$. In order to achieve a large dynamic range, the background will ideally be set to be close to the maximum possible value, i.e. $N_I \approx N_{sat}$. This leads to the brightfield signal-to-background-noise ratio of

$$SBNR_{BF} \approx \sqrt{QE \cdot N_{sat}} \cdot \kappa_{BF} \tag{5}$$

The darkfield case follows in a similar way. As mentioned above, illumination irradiance can be chosen larger than in the brightfield case, e.g. so large that the strongest scattering signal just reaches the sensor saturation. We here consider this by a *boost factor* $f_b = S_I/S_{sat} \geq 1$.

For low irradiance, background noise is dominated by the camera noise, leading to a SBNR of

$$SBNR_{DF} \approx \frac{QE\, N_{sat}}{\sigma_{cam}} \cdot f_b \cdot \kappa_{DF} \,. \tag{6}$$

Typical matrix sensors have Full-Well-Capacities of $N_{sat} = 10\ \ldots\ 40\ ke^-$ charge carriers, a quantum efficiency in the range of $QE \approx 60\%$ and sensor noise of $\sigma_{cam} \approx 10\ \ldots\ 20\ e^-$, for a common integration time. We arrive at SBNR values of $SBNR_{BF} \lesssim 100 \cdot \kappa_{BF}$ for brightfield, and of $SBNR_{DF} \lesssim 2000 \cdot f_b \cdot \kappa_{DF}$ for darkfield, respectively.

We can divide the influencing factors into the sensor properties on the one side, and the optical properties on the other side. The latter are determined by the imperfection scattering, the size and location of the imaging aperture and a possible boost factor for darkfield configuration. Brightfield and darkfield $SBNR$ are then compared by

$$\frac{SBNR_{DF}}{SBNR_{BF}} = \frac{\kappa_{DF} f_b}{\kappa_{BF}} \cdot \frac{\sqrt{QE\, N_{sat}}}{\sigma_{cam}} \quad . \tag{7}$$

Modern sensors are designed with large Full-Well-Capacity, high quantum efficiency and low sensor noise. From the sensor viewpoint alone, darkfield yields a more than 10 times better $SNBR$ than brightfield.

Note that the above estimation is only valid as long as the image of an imperfection completely covers at least one pixel. When the area A_{imp} of this image is smaller than the pixel area A_{pix}, size can only be estimated radiometrically. In such a case, the remainder of the pixels is exposed to the background irradiance and both scattering magnitudes need to be corrected $\kappa \rightarrow A_{imp}/A_{pix} \cdot \kappa$. For scratches, this ratio is proportional to the scratch width $A_{imp}/A_{pix} \sim w_{scratch}$, while for digs or other almost circular imperfections, the area ratio decays faster with their diameter $A_{imp}/A_{pix} \sim r_{dig}^2$: Small digs will be harder to detect than small scratches.

We can summarize that apart from the scattering magnitudes, there is a strong advantage for darkfield observation. The scattering magnitudes are determined by the individual imperfection and the numerical aperture of the imaging system. The smaller darkfield scattering magnitude may be balanced by larger illumination irradiance. On the other hand, the darkfield signal is sensitive to the angular spectrum of the illuminating radiation, and of the scattering distribution. As consequence, the pose between illumination direction, the imperfection and the imaging optics are important, whereas the brightfield setup is quite robust in this respect. In order to capture the maximum scattering radiance in darkfield with a fixed camera position, one can alter the illumination direction instead.

4. CAMERA DESIGN

4.1 Sensor

As mentioned above, each pixel should cover 5µm on the sample. With a sample diameter of 50 mm, this means that images with about 100 Megapixels are required. A straightforward approach is to use standard digital cameras with matrix sensors of moderate resolution of few Megapixels and to record several patches of smaller field of view4,5,6,17. These patches can be stitched together by software to form an image of the complete sample. The advantage is that this can be realized with standard technology, e.g. with a microscope equipped with a xy-translation stage. However, the required stop-and-go motion is quite time consuming and image-stitching may be problematic in some cases.

Another option is to use line scan cameras, which are commercially available with even more than 10k pixels. With such a camera, the sample has to be scanned in one direction, for example by rotation or linear transport under the scan line. This motion also takes a bit of time, but the resulting images can have unsurpassed resolution in terms of pixel numbers. Such a principle is utilized for a recently introduced AIS[7].

While this is a valid approach, we will instead follow the idea to inspect an optical element without any actuator, by a single snapshot, i.e. by using large matrix sensors. Recently, matrix sensors with 40 Megapixel and more have become commercially available, both in CCD and in CMOS technology. Camera bodies with these sensors are also already offered. Available sensors with 4000 … 7000 pixels in the short sensor dimension may allow the inspection of lenses with 20 … 35 mm diameter. Depending on sensor technology, pixel sizes range between 2.5 µm and 10 µm.

Note that from the sensor side, resolution is not only limited by pixel dimensions. Moreover, crosstalk between pixels can occur due to different physical processes. Pixel crosstalk, however, will be ignored here. Also, for every individual effect which limits system resolution, the same benchmark of 5 µm will applied in the following discussion. If all those effects come together, the resulting resolution will of course be considerably lower.

4.2 Imaging optics

With a given sensor pixel size and the required smallest imperfection size to be resolved, the optical magnification is set. In the present case we arrive at a magnification of $\beta \approx 1$, i.e. a macro lens. Remaining free parameters of the optical design are the F-number (F/#) and the focal length, from which follows the object side numerical aperture NA.

Diffraction will limit spatial resolution in the image, e.g. the Airy disc should not be larger than a sensor pixel. In order to be less limited by diffraction, larger pixel sizes are favorable. Concerning the lens aperture, a large NA, consequently a small F/# needs to be chosen. However, the effect of lens aberrations increases with smaller F/#, so that a compromise needs to be found. High quality lenses with small aberrations will allow smaller F-numbers. The overall resolution performance of a particular lens can be taken from its modulation transfer function (MTF). In contrast to other applications, geometric distortion and vignetting are of less importance for the present case. If necessary, both can be corrected by appropriate image processing.

4.3 Depth of Field

The choice of a large imaging aperture has the consequence of a small depth of field (DOF). Again, small sensor pixel sizes have a negative effect in resulting in smaller DOF values. For instance, the choice of a sensor with a pixel size of 5 µm and an aperture of F#= 2.8, the resulting DOF is less than 60 µm. Even when inspecting optical flats, this already requires precise focusing and precise adjustment of the sample under test. The inspection of curved surfaces, however, will not be possible for small radii of curvature. Even within a diameter of 25 mm, this DOF would cover only lenses with a radius of curvature of 330 mm.

Figure 7: Image of a scratch on a plane reference target, tilted by 45° (darkfield illumination). Top: single image with limited DOF. Bottom: result of focus stacking, covering a 'sag' of 20 mm.

Fortunately, there are a number of technologies to attain an extended depth of field. Some are related to methods to register the full surface profile in 3D (like photogrammetry, pattern projection, deflectometry, depth from focus), which however may be expensive in terms of hardware and may not always be working on glass surfaces. Other methods alter the optical process of image creation, e.g. by recording the full wavefront (light field cameras, digital holography) or by modifying the point spread function of the imaging system (wavefront coding).

A rather simple and wide-spread method is focus-stacking (related to the mentioned depth-from-focus): a stack of images is taken while shifting the focused object plane along the optical axis through the depth of the sample. From each image, only the focused areas are selected by appropriate filtering. These focused areas are combined to a single image, now showing the whole object with an artificially extended depth of field (see Figure 7)[18]. Satisfying results can already be achieved by taking only a small number images. True that this method is not really compatible with the initial idea of

inspecting with a single snapshot. Still it may serve as example what is possible and how even curved surfaces with a larger sag can be inspected with limited effort.

5. ACCEPTANCE AND REFERENCES

The discussion so far has shown that suitable AIS for surface imperfections can technically be realized. However, such systems also need acceptance, when being introduced into manufacturing environments. Part of the acceptance will be a validation, in order to confirm that the grading is 'correct'. This is in general tested by comparison to a suitable reference.

ISO 10100-7 defines grading on the basis of the geometrical size of the imperfections. In principle, the geometric extension could be measured rather precisely in microscope images. However, a close-up of real-world imperfections reveals that they may have rather complex shapes (see Figure 8 for a dig, or [15] for images of scratches). It is not necessarily clear, where the effective boundary of an imperfection is located. And it is not well defined, how to measure its area or width, e.g. by using the precise contour, a convex hull, or a bounding box.

Figure 8: Microscope image of a dig

Another reference could be given by ISO14997, e.g. by comparison to the appraisal of human operators. This standard is based on the visual appearance, which strongly depends on the optical setup. With the comparison to one or more human inspectors, subjectiveness comes into play, and possible dependences on the particular operator. When using this approach in an acceptance procedure for an AIS, more than one operator should be involved and tests should be repeated. This gives some insight in the variance of human grading, and a benchmark for possible deviations between automatic and human grading. Do not expect the deviations between AIS and a particular operator to be smaller than the deviations between different inspectors.

The application described here is not exactly a measurement (even though ISO 10100-7 refers to measurable quantities). The grading bins described in the standard documents are relatively large, so that it is questionable if the performance of such an AIS is adequately described in terms of measurement uncertainty. With respect to the few grading bins that are of practical importance in a real production, one may instead regard an AIS as a classification system. A proposal for the performance determination of classifying systems has been proposed elsewhere[19].

In terms of cosmetic part quality, the (radiometric) visibility of an imperfection is related to the practical demands. The MIL-standard indeed refers to visibility, but has the problem that it is based on subjective comparison to very specific reference plates. Even worse, there is no reproducible way to fabricate those plates, which today trace back to a master plate[20]. On the other hand, the ISO 10110-7 appears to have the advantage to be based on reproducible quantities, namely lateral geometric extensions, but these quantities do not have a stringent connection to visibility.

With AIS coming into play there will be much more degrees of freedom in designing the optical setup. One is no longer restricted to the resolution, aperture and working distance of the human eye. Moreover, wavelength spectrum and angular spectrum of the illumination have been shown to also have impact on the scattering distribution and hence on the detectability and visibility of imperfections. Nevertheless, these parameters are only weakly defined in the present standard documents. Hence, the community has to take care that the practical introduction of AIS will not be impeded by insufficient references and standards.

6. CONCLUSION

It has been outlined that modern machine vision hardware allows to build camera-based automatic inspection systems (AIS) for surface imperfections on precision optical elements. One critical point is to achieve a sufficient spatial resolution necessary to detect even small imperfections on larger samples, leading to requirements for the image sensor and the imaging optics.

On the sensor side, there is a basic choice between line scan and matrix cameras. Line scan cameras require motion of the sample for the scanning process, but do provide excellent resolution. In order to avoid motion and to inspect a sample by a single snapshot, state-of-the-art matrix sensor cameras may be utilized. In combination with a high-quality imaging optics, imperfections in the range of 10 µm size may be resolved on a sample with around 30 mm diameter.

One indirect consequence of the high resolution is the limited depth of field, leading to problems in inspecting curved surfaces. A number of technologies are available for countermeasures. The simple and proven technique of focus-stacking has been demonstrated in order to achieve an extended depth of field – however with the price of mechanical motion.

The detectability of imperfection strongly depends on the illumination conditions. There are good reasons to utilize darkfield illumination, because then the signal contrast, as well as the signal-to-background-noise ratio (SBNR) can be better than in brightfield conditions. In this context, the quantity SBNR has been introduced as a measure for detectability by image processing algorithms. The drawback of darkfield is that the direction of maximum radiance, scattered by an imperfection, is almost unpredictable. In order not to move the camera around, one can use several illumination directions, requiring good optical system design to fully exploit the demonstrated potential of darkfield.

The success of AIS in real manufacturing environments does not only depend on technical design aspects. One important topic in acceptance is the validation that AIS deliver correct grading results. Validation is mostly based on comparison to a reference, leading to a particular problem in the present case. Grading, as defined by ISO 10110-7, is related to the geometric extension of imperfections, which may not be well defined on a microscopic scale. Using ISO 14997 as reference instead results in a comparison to the grading by human operators, suffering from limited repeatability and reproducibility. Note that ISO 14997 (as well as MIL-PRF-13830B) refers to a visibility, which is not only determined by the lateral extension of an imperfection, but also by its depth and its microstructure.

7. ACKNOWLEDGEMENT

This work have been funded by the Central Research Funding Program of Darmstadt University of Applied Sciences under grant no. 41067000. Helpful discussions with the team at DIOPTIC GmbH are kindly acknowledged.

REFERENCES

[1] Young, M., “The scratch standard is only a cosmetic standard”, Proc. SPIE 1164, 185-190 (1989).
[2] Aikens, D. M., “The Truth About Scratch and Dig”, in International Optical Design Conference and Optical Fabrication and Testing, Technical Digest, paper OTuA2 (2010).
[3] Baker, L. M., [Metrics for high-quality specular surfaces], SPIE Press, Bellingham, USA (2004).
[4] Turchette, Q. and Turner, T., "Developing a more useful surface quality metric for laser optics", Proc. SPIE 7912, 791213 (2011).
[5] Turchette, Q. and Turner, T., "Automated Inspection of Optics using ISO Specifications”, Optics & Photonics News, July/August 2012, 15-16 (2012).
[6] Savvy Optics Corp., “SavvyInspector SIF-4E”, http://savvyoptics.com/files/SavvyInspectorTM_SIF4E_Technical_Sheet_OCT_2013doc.pdf (22.4.2016).
[7] DIOPTIC GmbH, Product data sheet “ARGOS”, http://dioptic.de/docs/ARGOS_product_sheet.pdf (22.4.2016).

[8] ISO 10110-7:2008, "Optics and photonics -- Preparation of drawings for optical elements and systems -- Part 7: Surface imperfection tolerances" (2008).
[9] ISO 14997:2011, "Optics and photonics -- Test methods for surface imperfections of optical elements" (2011).
[10] MIL-PRF-13830B, "Performance specification: optical components for fire control instruments: general specifications governing the manufacture, assemble, and inspection" (1997).
[11] Young, M., "Objective Measurement and characterization of scratch standards", Proc. SPIE 0362, 86 (April 5, 1983).
[12] Johnson, E. G. Jr., "Simulating the scratch standards for optical surfaces: theory", Appl. Opt. 22 (24), 4056-4068 (1983).
[13] Ha, T., Miyoshi, T., Takaya, Y., Takahashi, S., "Size determination of microscratches on silicon oxide wafer surface using scattered light", Prec. Eng. 27, 265-272 (2003).
[14] Feigenbaum, E., Raman, R. N., Nielsen, N. and Matthews, M. J., "Light scattering from laser-induced shallow pits on silica exit surfaces", Proc. SPIE 9632, 96320H (2015).
[15] Suratwala, T., Steele, R., Feit, M. D., Wong, L., Miller, P., Menapace J. and Davis, P., "Effect of rogue particles on the sub-surface damage of fused silica during grinding/polishing", J. Non-Cryst.Solids 354, 2023–2037 (2008).
[16] EMVA Standard 1288, "Standard for Characterization of Image Sensors and Cameras", Release 3.0, European Machine Vision Association (2010)
[17] Liu, D., Yang, Y., Wang, L., Zhuo, Y., Lu, C., Yang, L., Li, R., "Microscopic scattering imaging measurement and digital evaluation system of defects for fine optical surface", Opt. Commun. 278, 240–246 (2007).
[18] Image generated with the Matlab script "fstack.m" (version 1.0) by Yeh, Ch.-Y., Mathworks file exchange http://www.mathworks.com/matlabcentral/fileexchange/ (1.11.2015). Weblink no longer available.
[19] Neubecker, R., "Capability of classifying inspection systems", Proc. "Forum Bildverarbeitung 2014", http://dx.doi.org/10.5445/KSP/1000043608 (2014).
[20] Young, M., "Scratch-and-dig standard revisited", Appl. Opt. 25 (12), 1922-1929 (1986).

Lambda
www.lambdaphoto.co.uk
T: +44 (0)1582 764334